Predicting the Ultimate Tensile Strength of AISI 1045 steel and 2017-T4 aluminum alloy joints in a laser-assisted rotary friction welding process using Machine learning: a comparison with Response surface methodology

Germán Omar Barrionuevo
School of Engineering, Pontificia Universidad Católica de Chile
José Luis Mullo
School of Engineering, Pontificia Universidad Católica de Chile
Jorge Andrés Ramos-Grez (jramos@ing.puc.cl)
School of Engineering, Pontificia Universidad Católica de Chile

Research Article

Keywords: Rotary friction welding, Steel-aluminum joining, Ultimate tensile strength, Machine learning, Response surface methodology

Posted Date: March 22nd, 2021

DOI: https://doi.org/10.21203/rs.3.rs-344995/v1

Predicting the Ultimate Tensile Strength of AISI 1045 steel and 2017-T4 aluminum alloy joints in a laser-assisted rotary friction welding process using Machine learning: a comparison with Response surface methodology

Germán Omar Barrionuevo[1], José Luis Mullo[1,2], Jorge Andrés Ramos-Grez[1,3]

[1]Department of Mechanical and Metallurgical Engineering, School of Engineering, Pontificia Universidad Católica de Chile, Av. Vicuña Mackenna, 4860, Macul, Santiago, Chile
[2]Carrera de Tecnología Superior en Mecánica Automotriz, Instituto Superior Tecnológico Ciudad de Valencia (ISTCV), Quevedo, Ecuador
[3]Research Center for Nanotechnology and Advanced Materials (CIEN-UC), Av. Vicuña Mackenna, 4860, Macul Santiago, Chile

E-mail address: jramos@ing.puc.cl

Abstract

Welding metal alloys with dissimilar melting points make conventional welding processes not feasible to be used. Friction welding, on the other hand, has proven to be a promising technology. However, obtaining the welded joint's mechanical properties with characteristics similar to the base materials remains a challenge. In the development of this work, several of the machine learning (ML) regressors (e.g., Gaussian process, decision tree, random forest, gradient boosting, and multi-layer perceptron) were evaluated for the prediction of the ultimate tensile strength (UTS) in joints of AISI 1045 steel and 2017-T4 aluminum alloy produced by rotary friction welding with laser assistance. A mixed design of experiments was employed to assess the effect of the rotation speed, friction pressure, and laser power over the UTS. Furthermore, the response surface methodology (RSM) was employed to determine an empirical equation for predicting the UTS, and contours maps determine the main interactions. A total of 48 specimens were employed to train the regressors; the 5-fold cross-validation methodology was used to find the algorithm with greater precision. The gradient boosting regressor (GBR) and Gaussian processes regressors present the highest precision with a less than 3% percentage error for the laser-assisted rotary friction welding process. The capability of the GBR exceeds the accuracy of the RSM with a coefficient of determination (R^2) of 90.90 versus 83.24 %, respectively.

Keywords: Rotary friction welding, Steel-aluminum joining, Ultimate tensile strength, Machine learning, Response surface methodology.

1. Introduction

Metal joining processes are an essential need for various industries. Proper selection of materials and procedures and safety and quality standards are important aspects in the manufacturing industry [1]. For the union of materials with different characteristics, conventional fusion welding is not feasible due to the difference between their melting points; besides, intermetallic compounds with brittle characteristics are generated [2]. Solid-state welding is a novel joining process in which two workpieces are joined under pressure, generating frictional heat, but at temperatures below the base materials' melting point [3]. Friction welding (FW) is a solid-state joining method that produces the coalescence of materials under a compression force when workpieces rotate or move in contact with each other, producing heat and plastically displacing the material creating a welding interface [4]. Filler metal, flux, and a shielding gas are not required in this process. Due to its versatility, FW has promising industrial applicability as a mass production process for joining metals [5].

Manufacturing processes in the transport and aeronautical industry require welded cylindrical elements with good mechanical properties, low specific weight, and good corrosion resistance [6]. Joining steels and other materials in fusion welding processes can have unexpected phase propagation, grain boundary corrosion, or generation of delta and sigma ferrite phases at the weld interface [7]. The use of steel and aluminum parts in rotating systems and steel structures requires the development of reliable, efficient, and economic joining processes. Therefore, it is necessary to take certain precautions, such as using heat

treatments or higher welding speeds, since, in this way, a certain homogeneity in the welding interface will be achieved [8]. Furthermore, the proper selection of the processing parameters influences the mechanical properties of the joints. F. F. Wang, Li, Li, & Varis [9] mention that during the conventional rotational friction welding (RFW) process, the heat generation is mainly determined by the rotation speed, the friction pressure, and the friction time. Thus, the heating energy is very limited, especially for thin shaft welding. Winiczenko et al. [10] reported that the FW joints' nature is rather adhesive than diffusive for a couple of weight heavy alloy with aluminum alloy. H. Wang, G. Qin, P. Geng, and X. Ma [11] reached a joint efficiency of 88 % by continuous drive friction welding at a low friction time and high upset pressure.

Yilmaz, Çöl & Acet [12] applied a preheat of approximately 900 ºC at the interface of a steel shaft joined to an aluminum alloy. They determined that the intermetallic layer's thickness depends linearly on the friction time's square root, which indicates that growth occurs by diffusion. W.-Y. Li, Yu, Li, Zhang, & Wang [13] developed a friction heat-assisted electric arc welding process to join austenitic stainless steel (21-4N) and martensitic stainless steel (4Cr9Si2) from 4 mm diameter valves, achieving short welding times, otherwise very difficult to achieve using a conventional friction welding process. When analyzing the thermo-mechanically affected area (TMAZ) and the heat-affected zone (HAZ), they found that the plasticized area turned out to be more uniform than that achieved with the conventional method. For aluminum-aluminum joints, Campanelli, Casalino, Casavola, & Moramarco [14] found that laser treatment induces higher microhardness values and lower longitudinal residual stress on the surface of the aluminum weld zone. Jabbari [15] showed that an increase in the preheating time leads to a decrease in the processing time. For joints of dissimilar materials, Kutsuna, Yamagami, Rathod, & Ammar [16] studied the laser's effect on a joint of low carbon steel and an AA5052 aluminum alloy. They found a uniform layer of intermetallic compounds $FeAl_2$, $FeAl_3$, and Fe_2Al_5, which are reduced by increasing welding speed. Therefore, laser preheating presents many advantages; it is possible to use lower rotational speeds and friction pressures, thus reducing total welding time. Laser-assisted friction welding (LAFW) has been implemented in friction stir welding (FSW), but in RFW, it has been seldom explored. Recently, Mullo, Ramos-Grez, & Barrionuevo [17] demonstrated that LAFW could increase the interlayer bonding thickness by a 4-fold, , accelerating the diffusion process by a 25% and thus increasing the UTS of aluminum-steel bars.

On the other hand, thanks to the increase in computational power and the development of new machine learning (ML) algorithms. ML has been employed to learn information directly from the data without relying on a predetermined model [18]. Supervised ML algorithms map a function from known input-output pairs to estimate relationships between them. Some of the commonly employed ML algorithms for regression task are artificial neural networks (ANN) or multi-layer perceptron (MLP) [19], decision tree (DTR) [20], support vector machines (SVM) [21], Gaussian process (GP), ensembled methods (EM), among others. EM combines several base estimators' predictions with a given learning algorithm to produce one optimal predictive model [22] and reduce overfitting risk [23]. Some of the commonly applied EM include bagging methods, random forests (RFR) [24], and boosting methods as AdaBoost and gradient boosting regressors. [25]. Boosting ML algorithms brings new opportunities for optimizing advanced manufacturing systems, converting weak algorithms to strong ones, and reducing bias and variance [26].

The applicability of ML in FW has been little explored, there are just a few publications about it, and most of them are concentrated in FSW [27]. Hartl, Vieltorf, Benker, & Zaeh [28] applied GP to predict the ultimate tensile strength (UTS) in 6082-T6 joints of aluminum alloy processed by FSW. They concluded that GP could replace the tensile test for known materials by applying GP. The idea of replacing destructive testing with ML looks promising; however, experimentation will always be necessary to corroborate the predictions. One of the advantages of ML is that it is capable of predicting highly non-linear processes, and its application could optimize experimental designs to save material consumption and reduce the number of trials. Zhang & Xu [29] compared GP, ANN, and response surface methodology (RSM) to predict the material removal rate during the electrical discharge diamond surface grinding of Inconel-718. They recommended combined approaches to reduce experimental trials. Alternatively, Winiczenko [30] applied a hybrid methodology combining RSM and genetic algorithm to optimize the FW process's UTS. He developed a quadratic equation for the UTS prediction as a function of the friction force, friction time, and upset force. The accuracy was determined by the coefficient of determination (R^2).

Therefore, this work's first objective is to evaluate different ML algorithms to determine which presents higher accuracy for predicting UTS in a laser-assisted rotary friction welding (LARFW) process. To achieve this goal, 48 joints of AISI 1045 steel and 2017-T4 aluminum alloy produced by LARFW were subjected to a uniaxial tensile test varying the rotation speed, friction pressure, and laser power during the welding process. Second, the RSM is applied to assess each study parameter's contribution, and statistical

significance in the UTS performance is determined, and contour maps characterize the significant interactions.

2. Materials and method

2.1 Laser-assisted rotary friction welding procedure

The rotary friction welding was done on AISI 1045 steel and AA 2017-T4 rod size 15 mm in diameter and 180 mm in length. The base materials' nominal chemical compositions after GEDOS (Glow Emission Optical Discharge Spectroscopy) analysis are reported in Table 1. The mechanical properties of the base materials are presented in Table 2.

Table 1. Chemical composition of the steel and aluminum alloys

Material	**Elements (wt%)**							
AISI 1045	Fe	C	Mn	Si	Cu	Al	P	S
	98.41	0.40	0.72	0.22	0.13	0.02	0.01	0.01
AA 2017	Al	Cu	Mg	Mn	Fe	Zn	Cr	Si
	92.92	4.25	1.58	0.84	0.34	0.04	0.01	0.002

Table 2. Mechanical properties of the steel and aluminum alloys

Material	**Tensile strength** (MPa)	**Yield strength** (MPa)	**Elongation** (%)	**Hardness** (HV)
AISI 1045	617-680	330-392	< 18	260-330
AA 2017	370-420	215-260	< 18	105-120

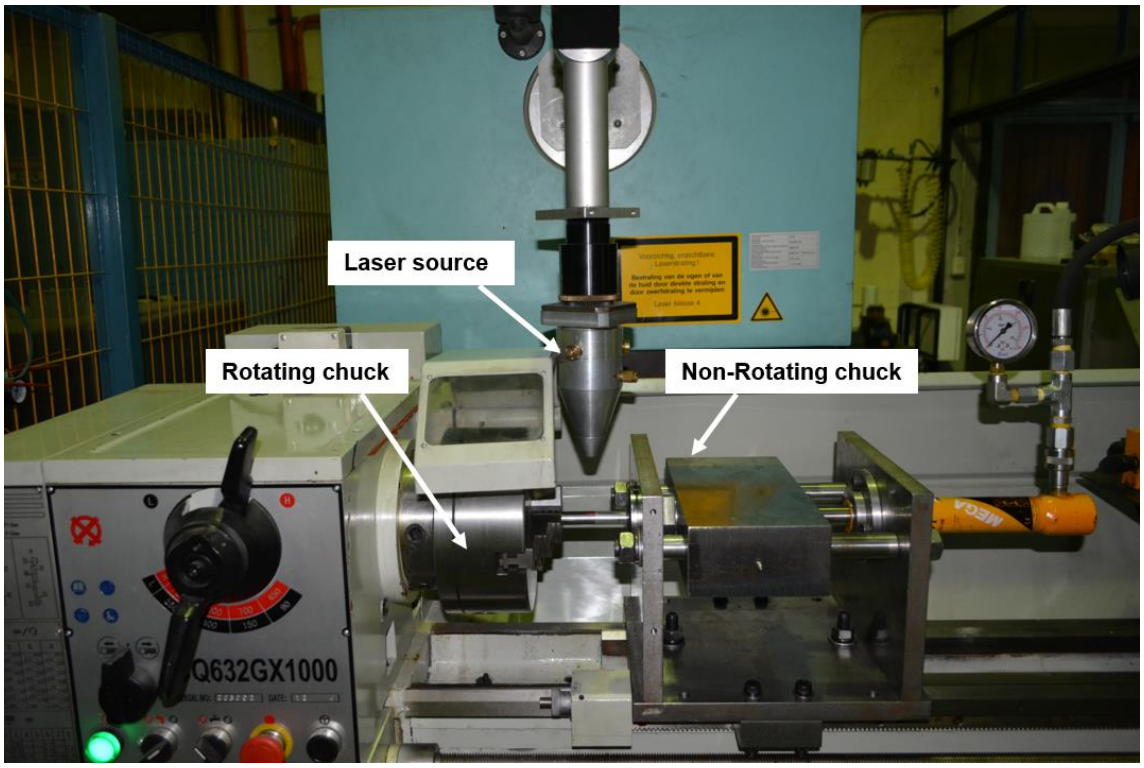

Figure 1. The experimental setup used for the laser-assisted rotary friction welding (LARFW)

A laser-assisted rotary friction welding (LARFW) procedure was employed, where a conventional lathe machine was adapted with a CO_2 laser (Oerlikon OPL3500) of 3.5 kW, a wavelength of 10.6 µm, and TEM_{00} (Figure 1). The lathe has 3 HP of power, 2000 RPM of rotation speed, and a distance between centers of 1000 mm. Furthermore, a hydraulic operated pressure system has been implemented that allows friction joints to be made at two pressure levels. The pressure mechanism consists of a 5-ton capacity hydraulic cylinder, which is driven by a 300cc hydraulic pump. The pressure mechanism also has a pressure gauge that allows visualizing the friction and forging pressures.

The joining process consists of preheating the steel rod for 40 seconds; the friction process starts until the rotational speed (N) is reached at 1600/1800 rpm, and then the axial friction pressure (14/21 MPa) was applied by the hydraulic mechanism until achieving forge for 60 seconds. Finally, the forging pressure was applied (42.1 MPa) for 40 seconds. The process parameters are listed in Table 3.

The ASTM E-8 standard was applied to test the ultimate tensile strength (UTS) of the welded specimens. The tensile test was performed using a universal testing machine (Instron 3368, Zwick) with a 50-kN capacity of 0.02 s^{-1} strain rate.

2.2 Design of experiments

The rotational speed and friction pressure were evaluated at two levels due to the experimental setup's limitations. The study's parameters and levels were selected by significance in the FW process reported in the literature [6],[11],[30],[31],[32]. The laser power was controlled at four levels, from no laser-assistance (0 W) to 600, 800, and 1000 W. The experiments were repeated three times for each set of parameters with a total of 48 produced specimens. The obtained results were processed statistically with Minitab 19®, where an analysis of variance (ANOVA) was conducted to analyze the main effects and their interactions to determine each factor's contribution. The main effects were defined as the mean response difference, which describes a single independent variable's action on the dependent variable (UTS).

Table 3. LARFW processing parameters and levels

ID	N (rpm)	FP (MPa)	LP (W)
S1	1600	14	0
S2	1600	21	0
S3	1800	14	0
S4	1800	21	0
S5	1600	14	600
S6	1600	14	800
S7	1600	14	1000
S8	1600	21	600
S9	1600	21	800
S10	1600	21	1000
S11	1800	14	600
S12	1800	14	800
S13	1800	14	1000
S14	1800	21	600
S15	1800	21	800
S16	1800	21	1000

2.1 Machine learning algorithms

Several of the most popular algorithms were used in this study. Decision tree, random forest, gradient boosting, Gaussian process, and multi-layer perceptron were accurately detailed in [33]. Extreme gradient

boosting regressor (XGBRegressor) is an optimized distributed gradient boosting library designed to be highly efficient, flexible, and portable [34]. The employed hyperparameters are described in Table 4.

Table 4. Hyperparameters selection for algorithms implementation

ML Algorithm	Hyperparameters
DTR	Maximum depth = 20
RFR	Number of trees in the forest = 2000, Maximum depth = 20
GBR	Number of trees = 2000, Learning rate = 0.1
XGBR	Number of trees = 2000, Maximum depth = 20, Learning rate = 0.1
GPs	Kernel = Radial based function (RBF), Noise level α = 0.001, Number of optimizers = 9
MLP	Hidden layers = 4, Activation function = relu, Number of iterations = 2000

The computations were performed in Google Colaboratory (Colab) environment using *Scikit-learn* and *XGBoost* libraries [35][36] on a CPU, which was an Intel® Core™ i7-7700HQ at 2.8 GHz, with 12 Gb of RAM installed.

2.2 Accuracy evaluation

A total of 48 samples were employed; the dataset was randomized and then split into training (80%) and testing (20%) portions. The input parameters were the rotation speed (N), friction pressure (FP), and laser power (LP), while the target value was the UTS. Before initiating the training process, the data were scaled using zero mean and unit variance. Five-fold Cross-validation (CV) was employed to avoid overfitting during the training process [23],[37]. To assess the prediction accuracy, Barrionuevo et al. [33] introduced an index of merit (IM), which combines multiple metrics to get a unique metric of the algorithms' accuracy. As the magnitude of the index approaches zero, the lower the error is achieved. The IM is calculated in the form of Eq. (1), whose components are the coefficient of determination (R^2), the mean squared error (MSE), and the mean absolute error (MAE) determined by equations (2), (3), and (4), respectively.

$$IM = \sqrt{(1 - R^2)^2 + MSE + (MAE)^2} \tag{1}$$

$$R^2 = 1 - \frac{\sum_i^N (y_i - \hat{y}_i)^2}{\sum_i^N (y_i - \bar{y}_i)^2} \tag{2}$$

$$MSE = \frac{1}{N}\sum_i^N (y_i - \hat{y}_i)^2 \tag{3}$$

$$MAE = \frac{1}{N}\sum_i^N |y_i - \hat{y}_i| \tag{4}$$

Once identified which algorithm presents the higher accuracy (lower IM), feature importance (FI) analysis was employed. FI assigns a score to input features based on how useful they are at predicting a target variable (UTS). Moreover, FI provides scores that help us provide obtain insight into the data, and the model can improve the efficiency and effectiveness of a predictive model on the predictions.

3. Results and discussion

3.1 Uniaxial tensile strength evaluation.

During the welding process, a flux formation around the aluminum rod was observed (Figure 2). The flash formation is mainly influenced by the friction pressure, leading to more significant deformation of the aluminum side, causing a greater flash effect due to the higher mechanical pressure [38]. After the RFW process, the specimens were prepared for the tensile test. Figure 3 shows the specimens after welding after machined for tensile test and after tensile test. It is possible to observe that the failure occurred at the welding interface.

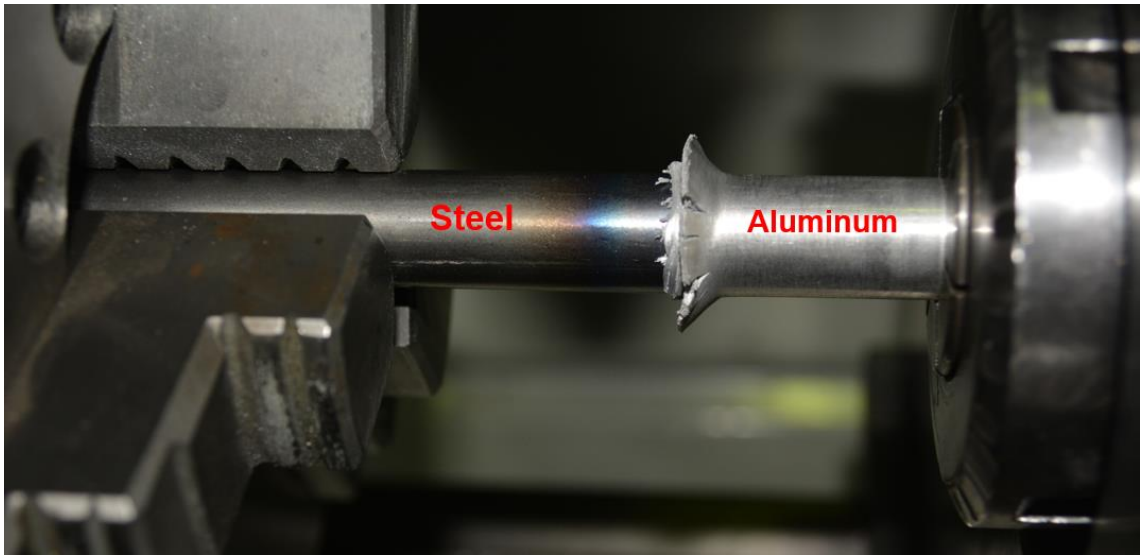

Figure 2. Flux formation around the aluminum alloy during rotary friction welding

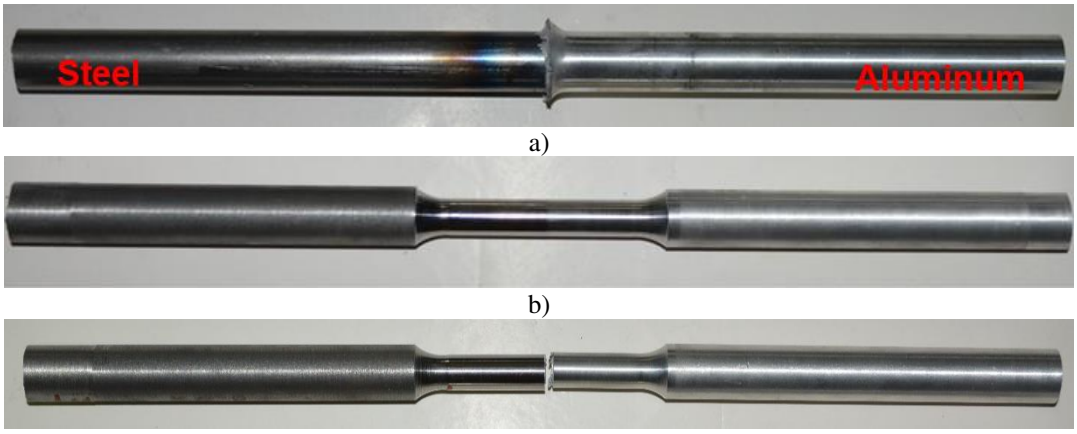

a)

b)

c)

Figure 3. Welded joint specimen: a) as processed, b) after machined for tensile test, c) after tensile test up to fracture

Figure 4 illustrates the range of UTS values obtained as a function of the process parameters. For the specimens manufactured by RFW without laser assistance (S1, S2, S3, and S4), the higher the friction pressure, the lower the UTS value. While for the LARFW process, the dominant parameter is laser power. The higher the laser power, the higher the UTS. For the RFW, the highest UTS value was 175.7 MPa in specimen S3. While for the LARFW, the highest UTS was 215.4 MPa.

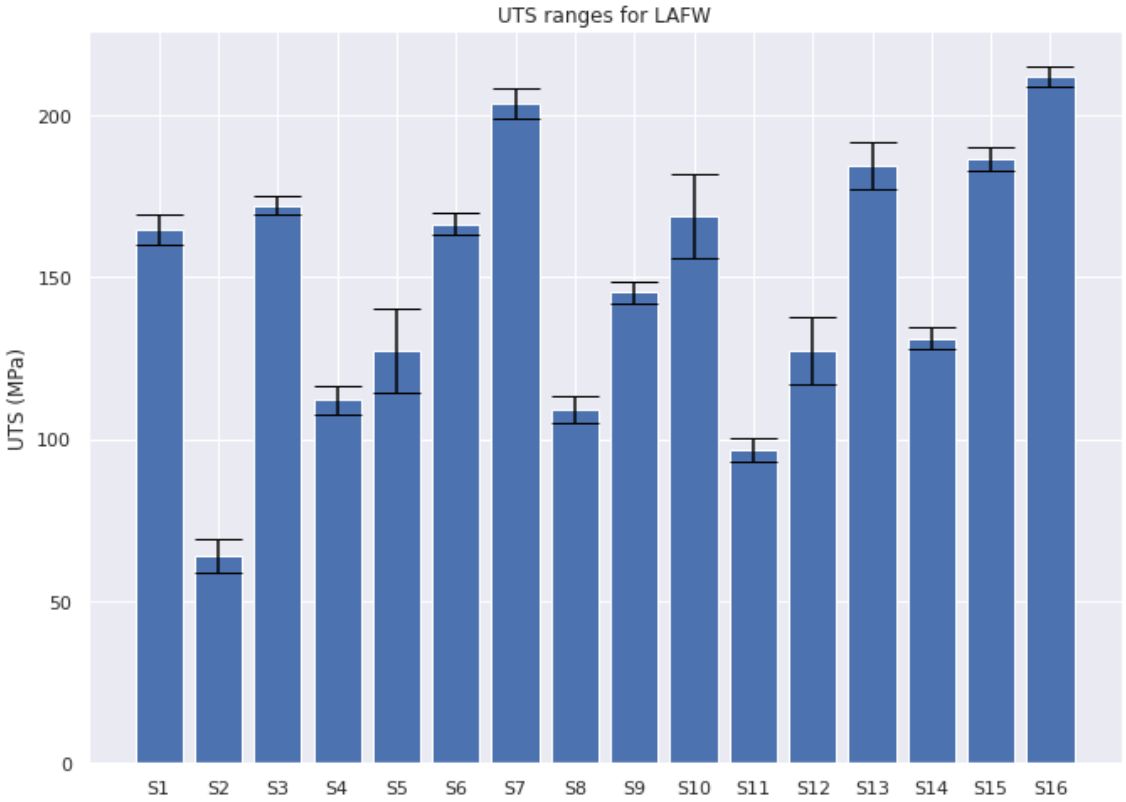

Figure 4. Boxplot of LARFW, UTS evaluation

3.2 Statistical analysis

Figure 5 shows a graph illustrating the main effects of the three factors. The main effects graph is used to observe how one or more factors influence a continuous response, here the UTS. For this study, the most statistical significative factor was the laser power. N and FP do not significantly affect the UTS value. Figure 6 summarizes the interaction effects between N, FP, and LP values for the UTS impact. The largest effect is observed for N and LP interactions, as indicated by the curve's slope.

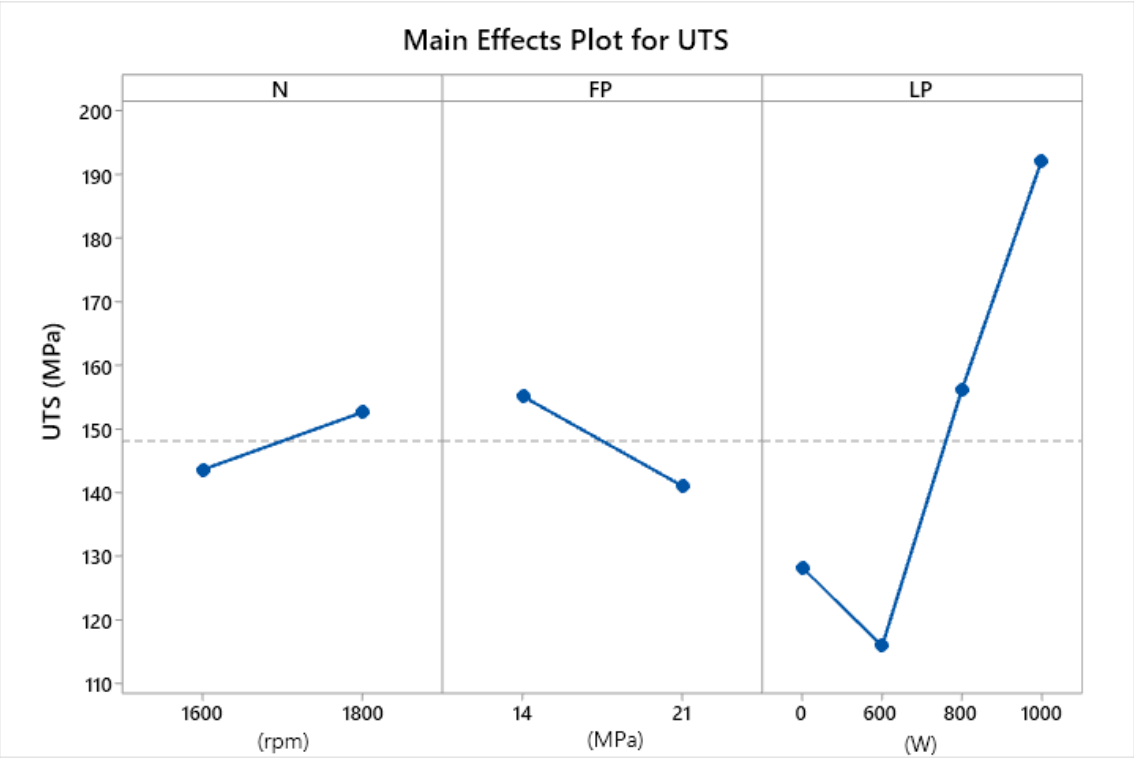

Figure 5. Main effects of experimental factors on the UTS

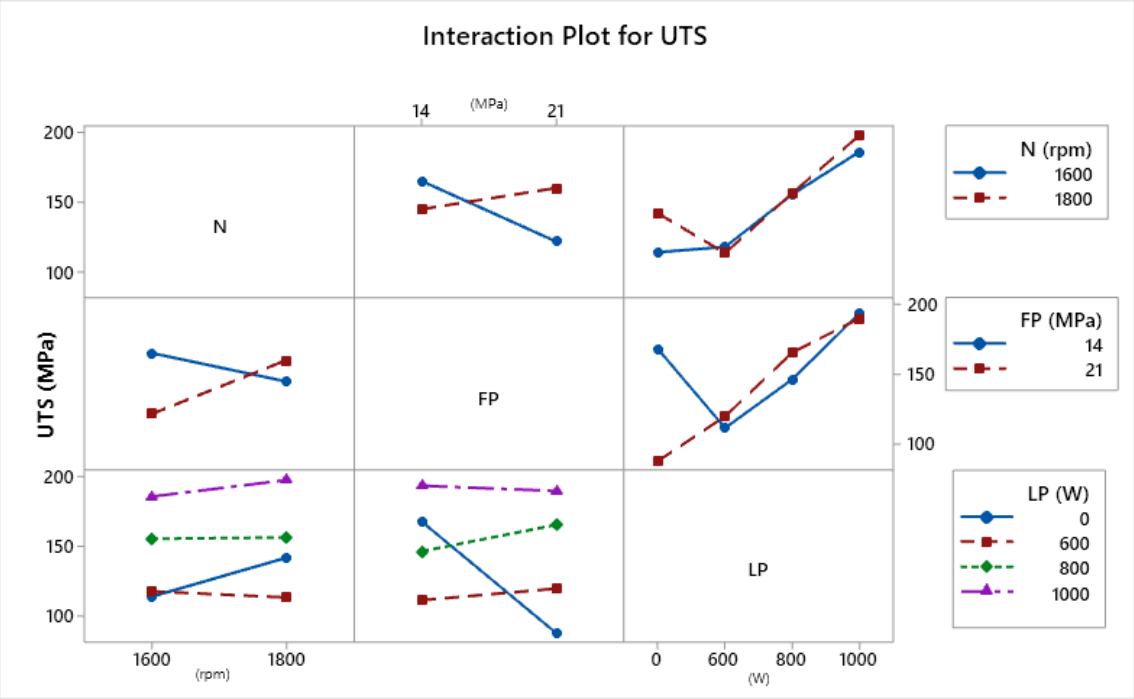

Figure 6. Interaction plot of factors on the overall UTS

The analysis of variance (ANOVA) is reported in Table 5. Each factor's significance is determined using the p-value; a p-value of less than 0.05 indicates that the factors or their interaction are statistically significant. Therefore, FP and LP and their interactions are statistically significant. Furthermore, the rotational speed does not play a significant role in LARFW, but it influences FP interaction. An empirical equation has been derived through the response surface methodology with a confidence level of 95 %.

Table 5. ANOVA results for ultimate tensile strength

Source	DF	Adj SS	Adj MS	F-Value	P-Value
Model	7	68614,0	9802,0	42,55	0,000
Linear	3	36334,8	12111,6	52,57	0,000
N	1	1397,3	1397,3	6,07	0,018
FP	1	6009,7	6009,7	26,09	0,000
LP	1	28927,7	28927,7	125,57	0,000
Square	1	19609,9	19609,9	85,12	0,000
LP*LP	1	19609,9	19609,9	85,12	0,000
2-Way Interaction	3	24776,1	8258,7	35,85	0,000
N*FP	1	10382,9	10382,9	45,07	0,000
N*LP	1	747,2	747,2	3,24	0,079
FP*LP	1	13646,0	13646,0	59,23	0,000
Error	40	9215,1	230,4		
Lack-of-Fit	8	7167,5	895,9	14,00	0,000
Pure Error	32	2047,6	64,0		
Total	47	77829,1			

Df: degrees of freedom, SS: sum of squares, MS: mean square, F, and P-value: statistics.

$$UTS = 1364 - 0.627\,N - 81.2\,FP - 0.178\,LP + 0.04202\,N \times FP - 0.000105\,N \times LP + 0.01288\,FP \times LP + 0.000199\,LP^2 \quad (5)$$

The goodness of the model given by the Eq. (5) is reported in Table 6. The coefficient of determination reaches a value superior to 83 % for the predicted UTS. Adjusted R^2 (R^2 (adj)), a modified version of R^2, adds precision and reliability by considering the impact of additional independent variables that tend to skew the results of R^2 measurements. S is measured in the UTS units representing the variation of how far the data values fall from the true response surface.

Table 6. RSM model summary

S	R^2	R^2 (adj)	R^2 (pred)
15,1782	88,16%	86,09%	83,24%

Figure 7, Figure 8, and Figure 9 show contour plots of the interaction between the welding parameters N, FP, and LP. Figure 7 shows that the highest UTS is obtained in the region where the highest laser power is combined with the highest friction pressure. In Figure 8, the interaction between speed and laser power is observed. It shows a quadratic response for the N as a function of LP; through the contour plot is possible to distinguish a range where the laser power achieves the lowest UTS (200-600 W). The interaction between rotational speed and friction pressure is depicted in the contour plot in Figure 9. In this case, the higher the speed and lower friction pressure produced the lowest UTS. While at the highest FP, and N the UTS performance was improved.

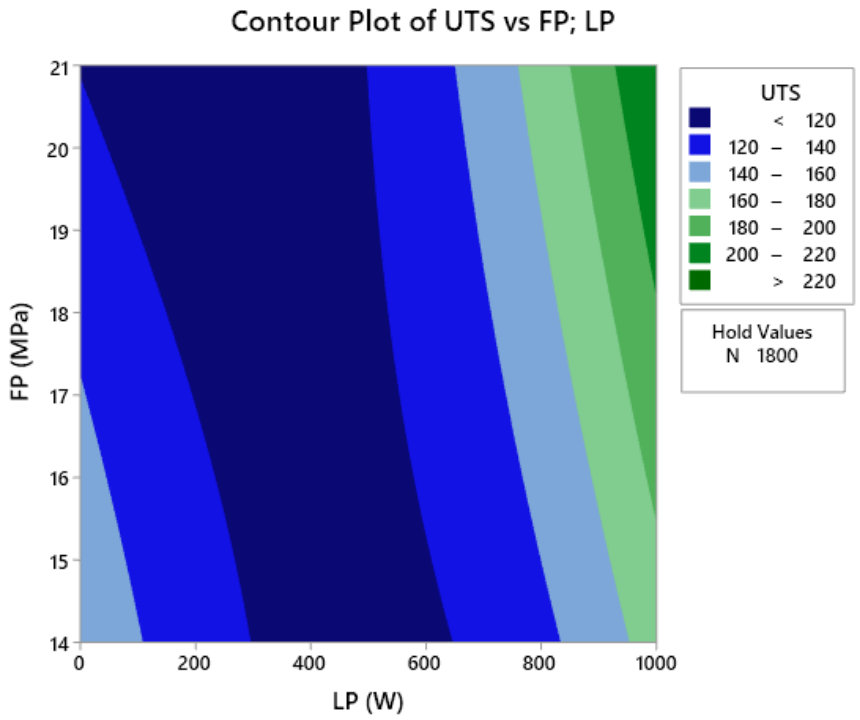

Figure 7. Contour plot of interaction between laser power and friction pressure

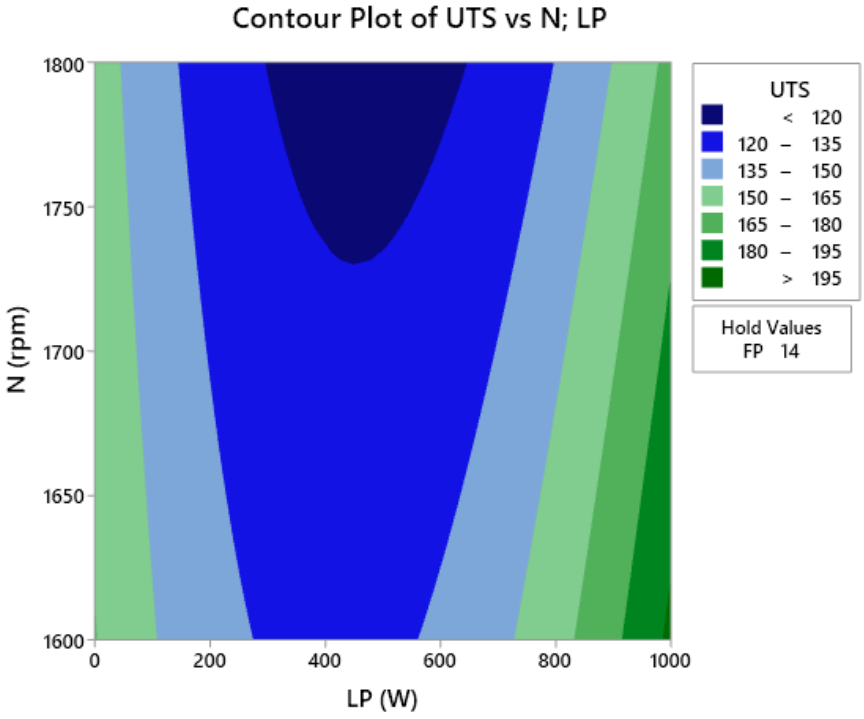

Figure 8. Contour plot of interaction between laser power and rotational speed

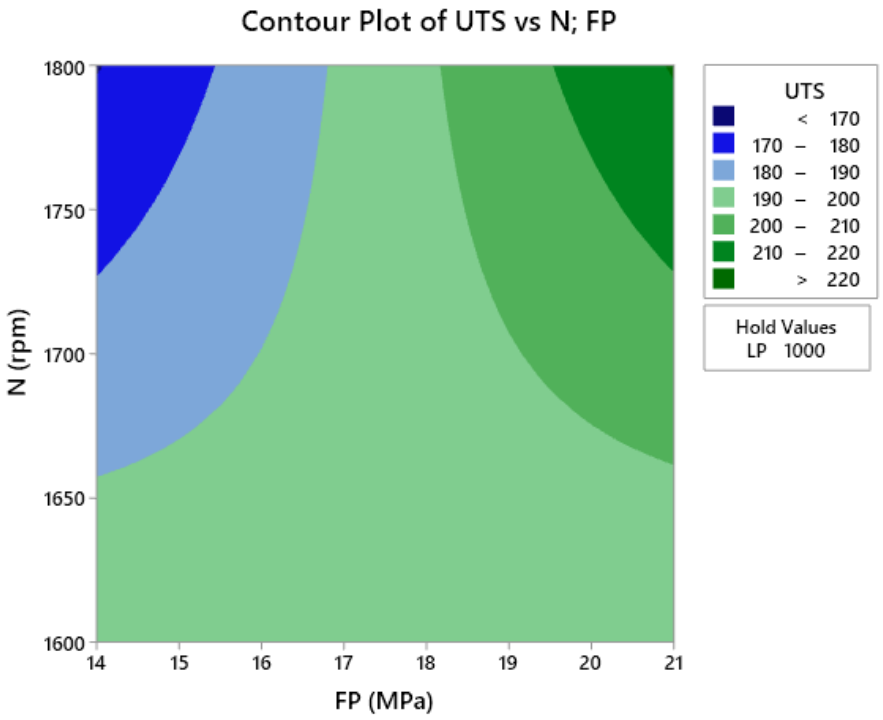

Figure 9. Contour plot of interaction between friction pressure and rotational speed

Additionally, a Pareto chart shows the standardized effect of the parameters, where the laser power contributes the most to the variability in the UTS response. The reference line on the chart indicates which effects are significant.

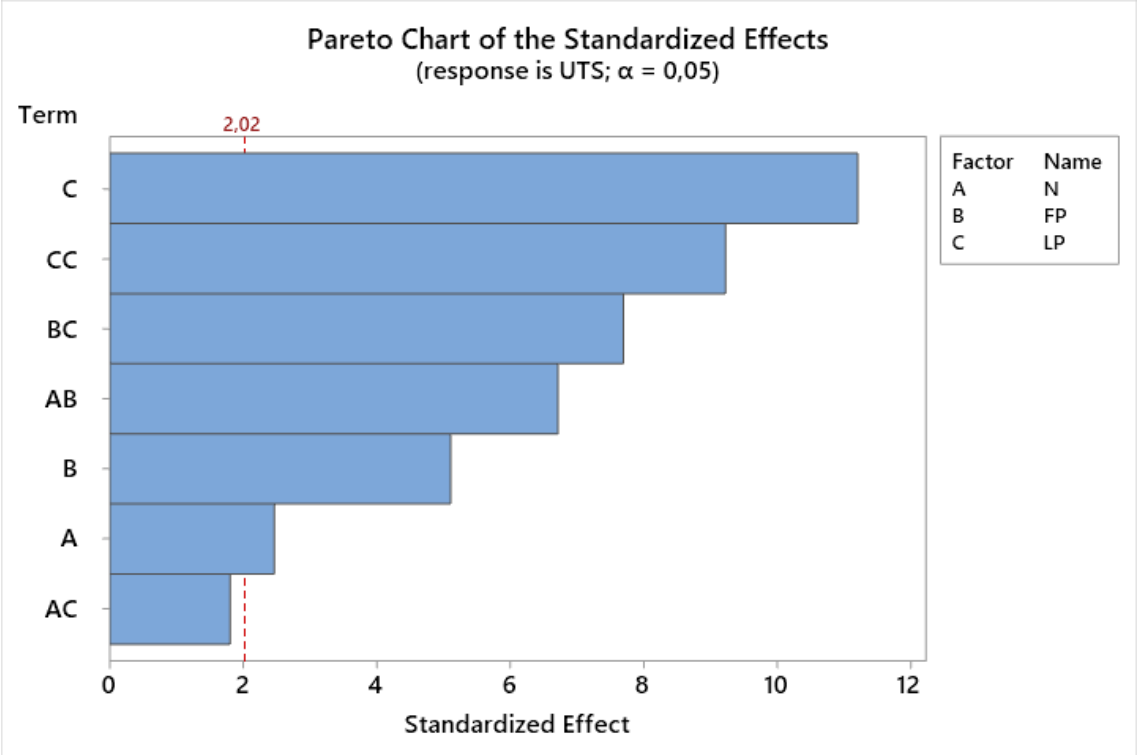

Figure 10. Pareto chart of the standardized effect

3.3 Machine learning evaluation

Figure 11 illustrates the ML algorithms' behavior for predicting the UTS; the vertical axis shows the predicted value and the measured value's horizontal axis, both were scaled to zero means. In Table 7 it is reported the metrics obtained for the CV and testing procedures. For the CV, GBR appears the most accurate algorithm with the highest R^2, the lowest RMSE, MAE, and the corresponding lowest IM. GPs also show good performance with low IM. The remaining algorithms show lower R^2 than GBR and GPs and higher RMSE and MAE, with IMs higher than 0.5345. For the testing dataset, almost every algorithm performance shows good accuracy; just the RFR shows poor accuracy, with the highest IM.

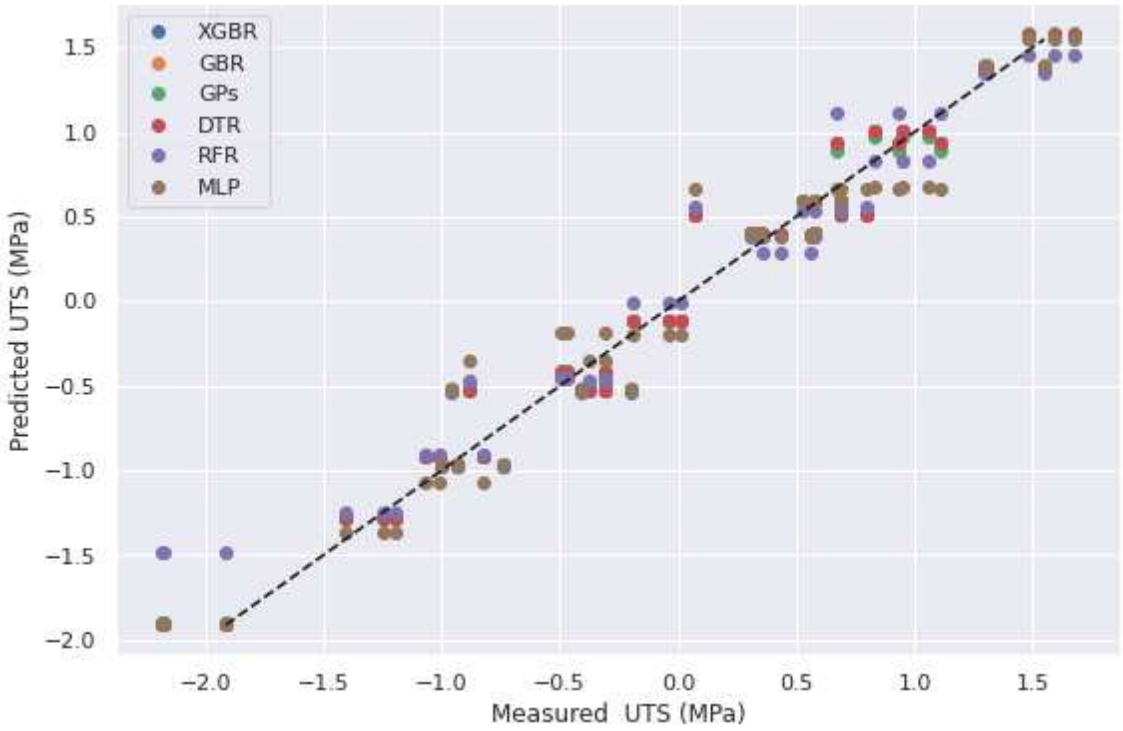

Figure 11. Scatter plot for comparing ML regressors accuracy in the UTS prediction.

Table 7. Performance of the ML algorithms employed to predict the UTS for the CV and testing dataset

	Cross-validation				**Testing**			
ML Algorithm	**R^2**	**RMSE**	**MAE**	**IM**	**R^2**	**RMSE**	**MAE**	**IM**
GBR	0.9091	0.0687	0.2049	0.3449	0.9759	0.1971	0.1825	0.2697
GPs	0.8339	0.1266	0.2424	0.4615	0.9761	0.1965	0.1804	0.2679
MLP	0.7986	0.1534	0.303	0.5345	0.9693	0.1975	0.1807	0.2694
DTR	0.7731	0.1758	0.2913	0.5586	0.9760	0.1975	0.1826	0.2701
XGBR	0.7716	0.1770	0.2917	0.5606	0.9758	0.1975	0.1831	0.2704
RFR	0.7568	0.1898	0.3064	0.5855	0.9200	0.3598	0.2635	0.4531

Figure 12 shows the performance during training and testing for the GBR algorithm. This observation provides insight into the algorithm's excellent performance for the UTS prediction in laser-assisted rotary friction welding.

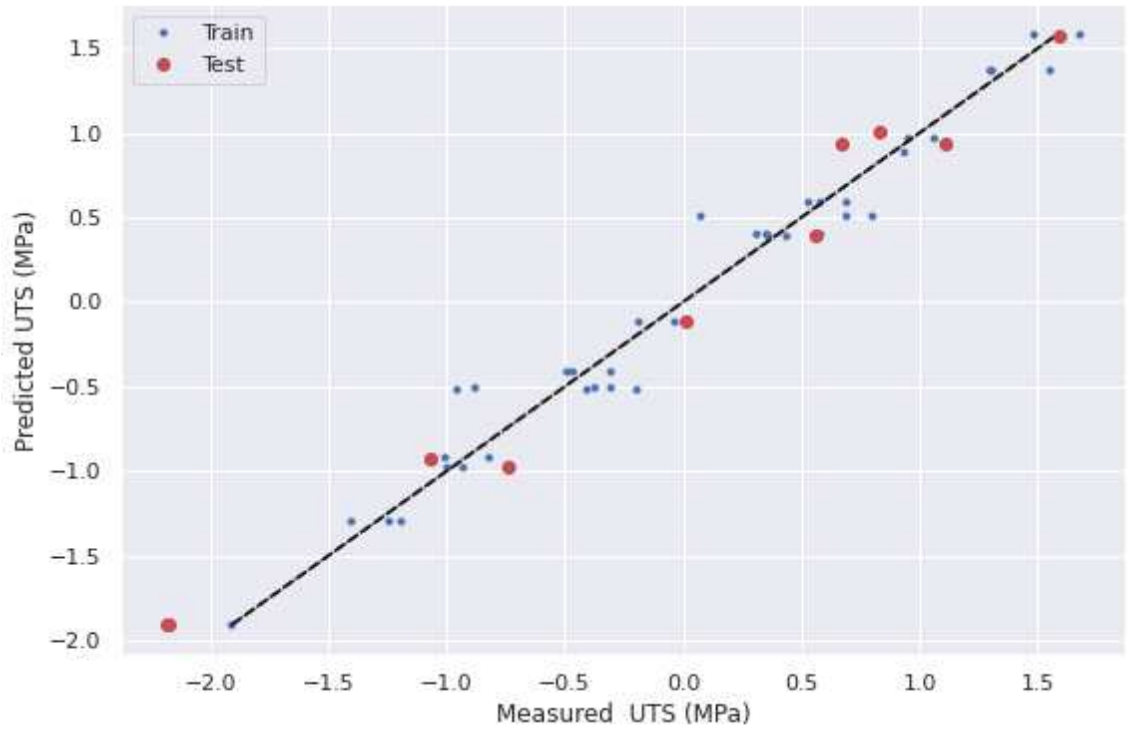

Figure 12. Scatter plot for accuracy evaluation of the GBR performance in the UTS prediction.

3.4 Feature important analysis.

Figure 13 shows the feature importance analysis, where the laser power represents the main factor for predicting the UTS. The rotation speed (Feature 0) represents less than 10% of the model predictivity, friction pressure (Feature 1) represents around 30%, while laser power appears the most significant parameter, with a score superior to 60% (Feature 2).

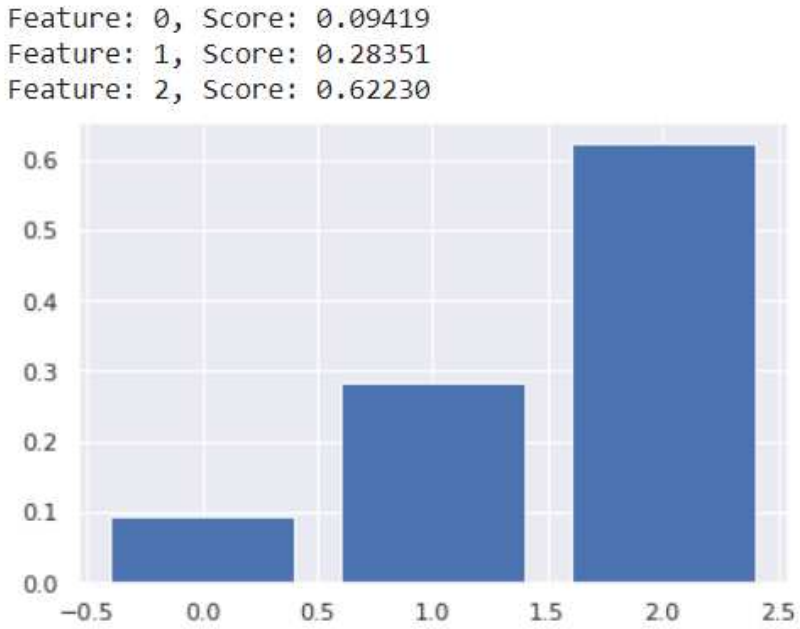

Figure 13. Feature importance analysis of the processing parameters in LARFW

The FI results agree with the Pareto chart, corroborating that the laser power represents the most statistically significant factor for the UTS prediction in laser-assisted rotary friction welding.

Conclusions

This paper evaluates several machine learning regressors to predict the UTS, resulting from a laser-assisted rotary friction welding process between 2017-T4 aluminum and AISI 1045 steel. The following conclusions can be drawn:

1) The application of the laser improves the ultimate tensile strength. For the conventional rotary friction welding process, there is an average UTS value of 119 MPa, while for the laser-assisted process, there is a UTS value of 152 MPa, which represents an increase of near to 28%. The range of values for UTS in RFW covers values from 64 to 175.7 MPa. For LAFW, there are values from 96.45 to 215.4 MPa.

2) The algorithms that better perform predicting the UTS were gradient boosting regressor and Gaussian process regressor, which show the highest coefficient of determination, the lowest root mean squared error, and the lowest mean absolute error.

3) The ML algorithms' accuracy was examined through the index of merit (IM), which appears as a robust estimator since it groups three metrics in one. The lower the IM, the more accurate the algorithm predicts the UTS.

4) The empirical Equation obtained through the response surface methodology explains 83.64 % of the UTS performance variation, denoting the importance of the laser power factor on the UTS prediction. It is important to note that this empirical relationship only represents this particular LARFW set up and materials system used.

5) The GBR algorithm outperforms the prediction capability of the RSM, obtaining a coefficient of determination (R^2) higher than the RMS value.

Acknowledgments

SENESCYT has founded this study through grant number ARSEQ-BEC-000329-2017. The authors also acknowledge the Research Center for Nanotechnology and Advanced Materials (CIEN-UC) and ANID FONDECYT #1201068 project and FONDEQUIP EQM160091 project.

Authors' contributions Germán Omar Barrionuevo: paper original idea, conceptualization, data curation, investigation, methodology, statistical analysis, writing–original draft and editing.

José Luis Mullo: literature review, design of experiments, experimental setup, and data generation, tensile testing, and manuscript proofread and valuable comments.

Jorge Andrés Ramos Grez: paper original conceptualization, close supervision and guidance during research process, index of merit formulation, critical advice, and manuscript proofread and funding.

Funding This study is financially supported by the SENESCYT grant no. ARSEQ-BEC-000329-2017 and ANID FONDECYT grant no. 1201068 project.

Data availability Source files are available in GitHub:
https://github.com/GermanOmar/LAFW/blob/master/LARFW_IJAMT.ipynb

Declarations

Ethics approval Not applicable.

Consent for publication All listed authors approve to publish.

Conflict of interest The authors have no competing interests.

References

[1] W. Li, A. Vairis, M. Preuss, and T. Ma, "Linear and rotary friction welding review," *Int. Mater. Rev.*, vol. 61, no. 2, pp. 71–100, 2016.

[2] K. P. Mehta, "A review on friction-based joining of dissimilar aluminum-steel joints," *J. Mater. Res.*, vol. 34, no. 1, pp. 78–96, 2019.

[3] W. Cai *et al.*, "A state-of-the-art review on solid-state metal joining," *J. Manuf. Sci. Eng. Trans. ASME*, vol. 141, no. 3, pp. 1–35, 2019.

[4] M. Maalekian, "Friction welding - Critical assessment of literature," *Sci. Technol. Weld. Join.*, vol. 12, no. 8, pp. 738–759, 2007.

[5] G. Ananda Rao and N. Ramanaiah, "Dissimilar metals AISI 304 steel and AA 2219 aluminium alloy joining by friction welding method," *Mater. Today Proc.*, vol. 19, pp. 902–907, 2019.

[6] G. L. Wang, J. L. Li, J. T. Xiong, W. L. Wang, P. Y. MA, and F. S. Zhang, "Study on the friction interface evolution during rotary friction welding of tube," *J. Adhes. Sci. Technol.*, vol. 33, no. 10, pp. 1033–1046, 2019.

[7] G. S. Chander, G. M. Reddy, and A. V. Rao, "Influence of Rotational Speed on Microstructure and Mechanical Properties of Dissimilar Metal AISI 304-AISI 4140 Continuous Drive Friction Welds," *J. Iron Steel Res. Int.*, vol. 19, no. 10, pp. 64–73, 2012.

[8] G. K. Padhy, C. S. Wu, and S. Gao, "Auxiliary energy assisted friction stir welding – Status review," *Sci. Technol. Weld. Join.*, vol. 20, no. 8, pp. 631–649, 2015.

[9] F. F. Wang, W. Y. Li, J. L. Li, and A. Vairis, "Process parameter analysis of inertia friction welding nickel-based superalloy," *Int. J. Adv. Manuf. Technol.*, vol. 71, no. 9–12, pp. 1909–1918, 2014.

[10] R. Winiczenko, O. Goroch, A. Krzyńska, and M. Kaczorowski, "Friction welding of tungsten heavy alloy with aluminium alloy," *J. Mater. Process. Technol.*, vol. 246, pp. 42–55, 2017.

[11] H. Wang, G. Qin, P. Geng, and X. Ma, "Interfacial microstructures and mechanical properties of friction welded Al/steel dissimilar joints," *J. Manuf. Process.*, vol. 49, no. November 2019, pp. 18–25, 2020.

[12] M. Yilmaz, M. Çöl, and M. Acet, "Interface properties of aluminum/steel friction-welded components," *Mater. Charact.*, vol. 49, no. 5, pp. 421–429, 2002.

[13] W.-Y. Li, M. Yu, J. Li, G. Zhang, and S. Wang, "Characterizations of 21-4N to 4Cr9Si2 stainless steel dissimilar joint bonded by electric-resistance-heat-aided friction welding," *Mater. Des.*, vol. 30, no. 10, pp. 4230–4235, 2009.

[14] S. L. Campanelli, G. Casalino, C. Casavola, and V. Moramarco, "Analysis and comparison of friction stir welding and laser assisted friction stir welding of aluminum alloy," *Materials (Basel).*, vol. 6, no. 12, pp. 5923–5941, 2013.

[15] M. Jabbari, "Effect of the Preheating Temperature on Process Time in Friction Stir Welding of Al 6061-T6," *J. Eng.*, vol. 2013, 2013.

[16] M. Kutsuna, N. Yamagami, M. J. Rathod, and H. Y. A. Ammar, "Laser roll welding for joining of low-carbon steels to aluminium alloys," *Weld. Int.*, vol. 20, no. 6, pp. 446–456, 2006.

[17] J. L. Mullo, J. Ramos-Grez, and G. O. Barrionuevo, "Effect of Laser Heat Treatment on the Mechanical Performance and Microstructural Evolution of AISI 1045 Steel-2017-T4 Aluminum Alloy Joints during Rotary Friction Welding," *J. Mater. Eng. Perform.*, 2021.

[18] S. M. Chelly and C. Denis, "Introducing Machine Learning," *Med. Sci. Sports Exerc.*, vol. 33, no. 2, pp. 326–333, 2001.

[19] I. Goodfellow, Y. Bengio, and A. Courville, *Deep Learning Adaptive Computation and Machine Learning*, vol. 1. 2016.

[20] H. K. Gianey and R. Choudhary, "Comprehensive Review On Supervised Machine Learning Algorithms," *Proc. - 2017 Int. Conf. Mach. Learn. Data Sci. MLDS 2017*, vol. 2018-Janua, pp. 38–43, 2018.

[21] S. Sun, Z. Cao, H. Zhu, and J. Zhao, "A Survey of Optimization Methods From a Machine Learning Perspective," *IEEE Trans. Cybern.*, pp. 1–14, 2019.

[22] N. Duffy and D. Helmbold, "Boosting Methods for Regression," *Theor. Comput. Sci.*, vol. 284, no. 1, pp. 67–108, 2002.

[23] A. Prieditis and S. Sapp, "Lazy overfitting control," *Lect. Notes Comput. Sci. (including Subser. Lect. Notes Artif. Intell. Lect. Notes Bioinformatics)*, vol. 7988 LNAI, pp. 481–491, 2013.

[24] A. Singh, N. Thakur, and A. Sharma, "A review of supervised machine learning algorithms," *Proc. 10th INDIACom; 2016 3rd Int. Conf. Comput. Sustain. Glob. Dev. INDIACom 2016*, pp. 1310–1315, 2016.

[25] O. Sagi and L. Rokach, "Ensemble learning: A survey," *Wiley Interdiscip. Rev. Data Min. Knowl. Discov.*, vol. 8, no. 4, pp. 1–18, 2018.

[26] Z.-H. Zhou, *Ensemble Methods Foundations and Algorithms*. 2014.

[27] B. Eren, M. A. Guvenc, and S. Mistikoglu, "Artificial Intelligence Applications for Friction Stir Welding: A Review," *Met. Mater. Int.*, vol. 27, no. 2, pp. 193–219, 2020.

[28] R. Hartl, F. Vieltorf, M. Benker, and M. F. Zaeh, "Predicting the ultimate tensile strength of friction stirwelds using gaussian process regression," *J. Manuf. Mater. Process.*, vol. 4, no. 3, 2020.

[29] Y. Zhang and X. Xu, "Predicting the material removal rate during electrical discharge diamond grinding using the Gaussian process regression: a comparison with the artificial neural network and response surface methodology," *Int. J. Adv. Manuf. Technol.*, pp. 1527–1533, 2021.

[30] R. Winiczenko, "Effect of friction welding parameters on the tensile strength and microstructural properties of dissimilar AISI 1020-ASTM A536 joints," *Int. J. Adv. Manuf. Technol.*, vol. 84, no. 5–8, pp. 941–955, 2016.

[31] Y. Liu, H. Zhao, Y. Peng, and X. Ma, "Microstructure characterization and mechanical properties of the continuous-drive axial friction welded aluminum/stainless steel joint," *Int. J. Adv. Manuf. Technol.*, vol. 104, no. 9–12, pp. 4399–4408, 2019.

[32] E. Taban, J. E. Gould, and J. C. Lippold, "Dissimilar friction welding of 6061-T6 aluminum and AISI 1018 steel: Properties and microstructural characterization," *Mater. Des.*, vol. 31, no. 5, pp. 2305–2311, May 2010.

[33] G. Barrionuevo, J. Ramos-Grez, M. Walczak, and C. Betancourt, "Comparative evaluation of supervised machine learning algorithms in the prediction of the relative density of 316L stainless steel fabricated by selective laser melting," *Int. J. Adv. Manuf. Technol.*, 2021.

[34] J. Deng, Y. Xu, Z. Zuo, Z. Hou, and S. Chen, "Bead Geometry Prediction for Multi-layer and Multi-bead Wire and Arc Additive Manufacturing Based on XGBoost," pp. 125–135, 2019.

[35] F. Pedregosa *et al.*, "Scikit-learn: Machine Learning in Python," *J. Mach. Learn. Res.*, vol. 19, no. 1, pp. 29–33, 2011.

[36] L. Buitinck *et al.*, "API design for machine learning software: experiences from the scikit-learn project," pp. 1–15, 2013.

[37] I. Baturynska and K. Martinsen, "Prediction of geometry deviations in additive manufactured parts: comparison of linear regression with machine learning algorithms," *J. Intell. Manuf.*, 2020.

[38] E. Taban, J. E. Gould, and J. C. Lippold, "Dissimilar friction welding of 6061-T6 aluminum and AISI 1018 steel: Properties and microstructural characterization," *Mater. Des.*, vol. 31, no. 5, pp. 2305–2311, 2010.

Figures

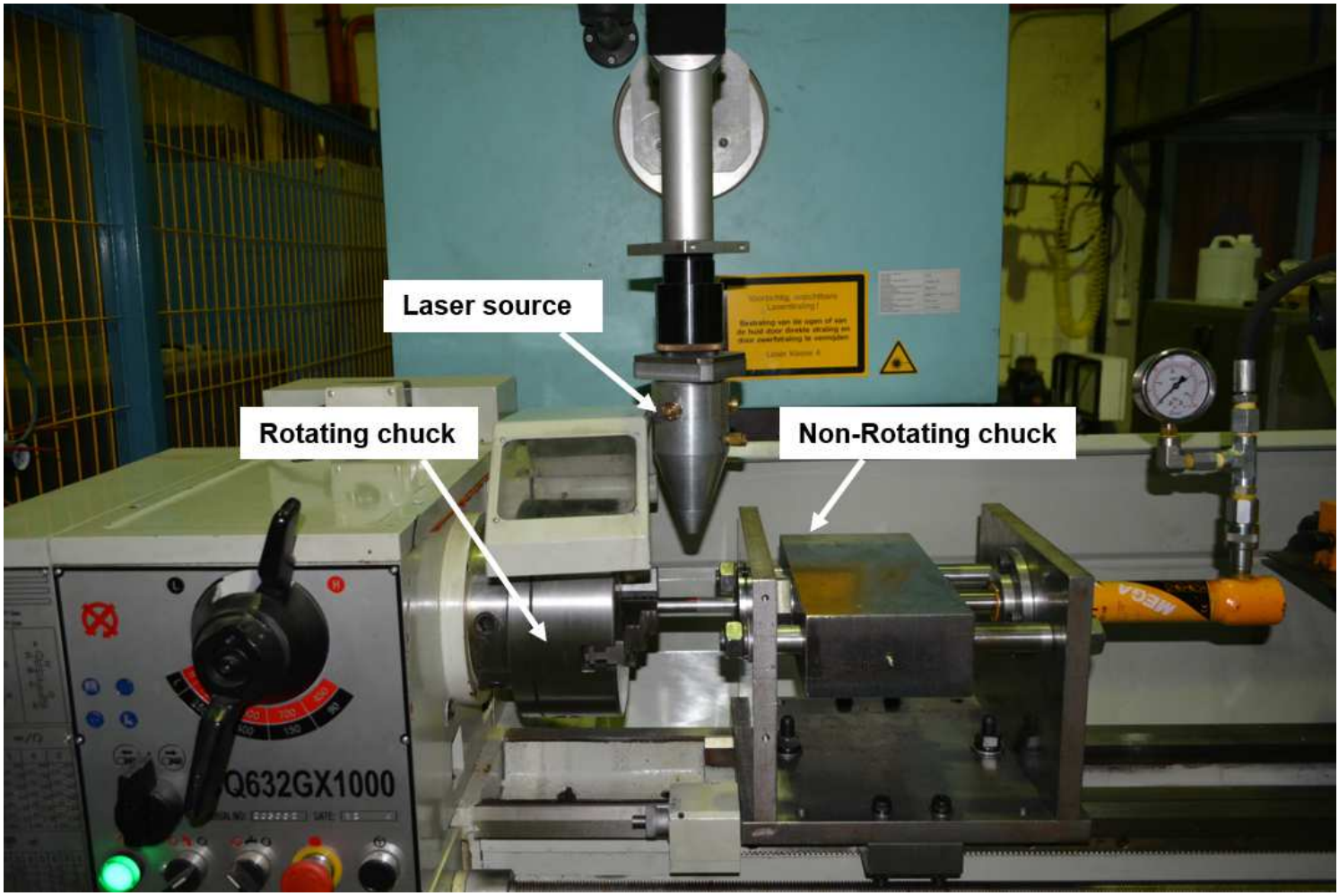

Figure 1

The experimental setup used for the laser-assisted rotary friction welding (LARFW)

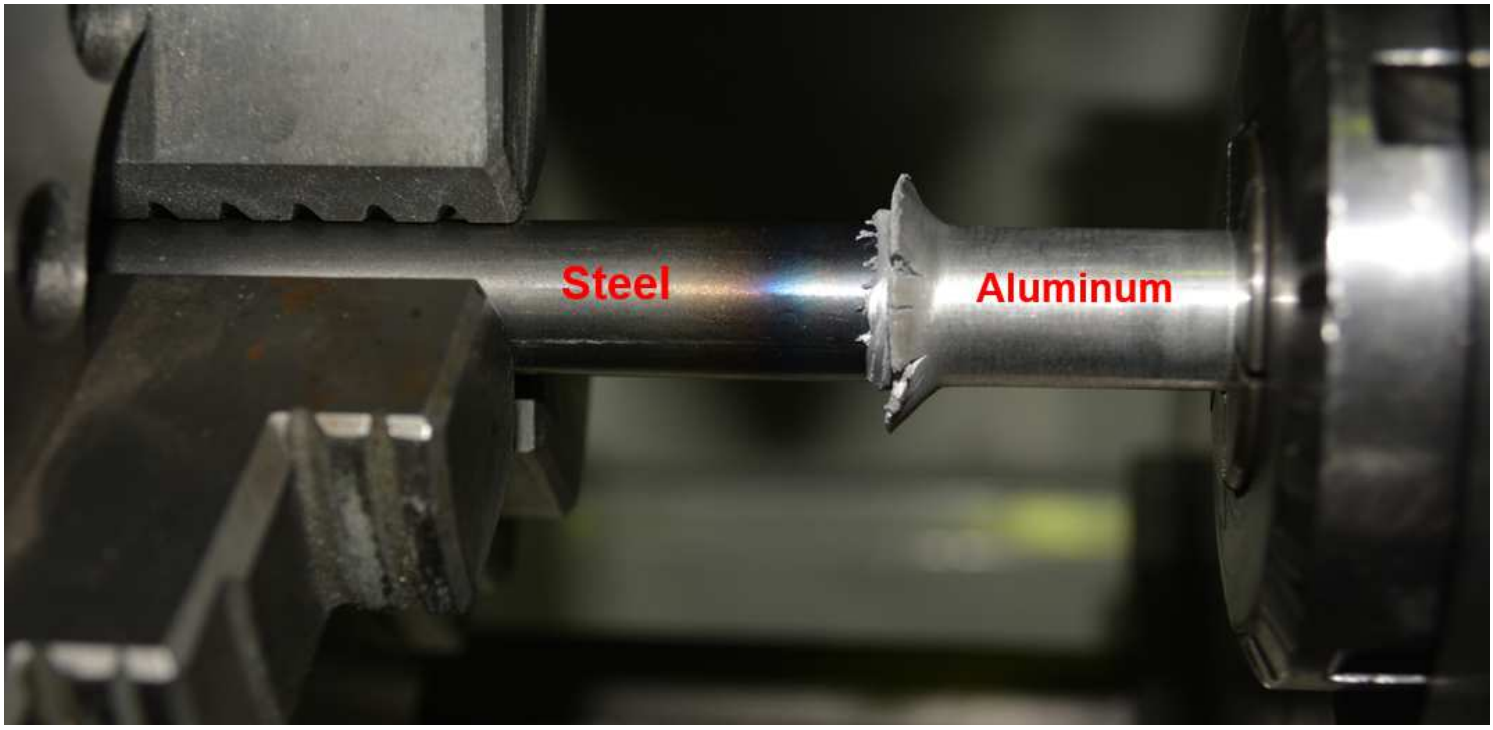

Figure 2

Flux formation around the aluminum alloy during rotary friction welding

Figure 3

Welded joint specimen: a) as processed, b) after machined for tensile test, c) after tensile test up to fracture

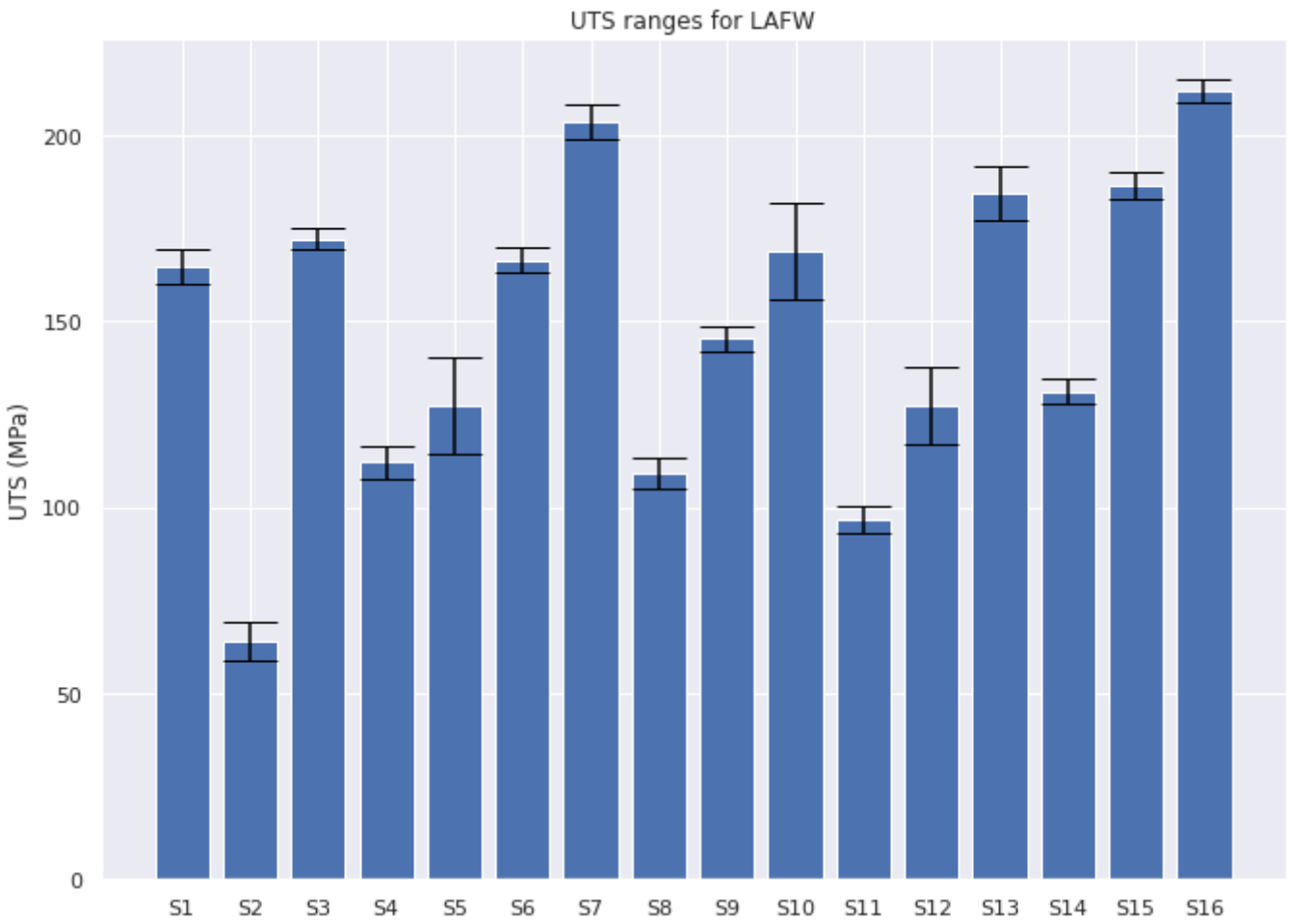

Figure 4

Boxplot of LARFW, UTS evaluation

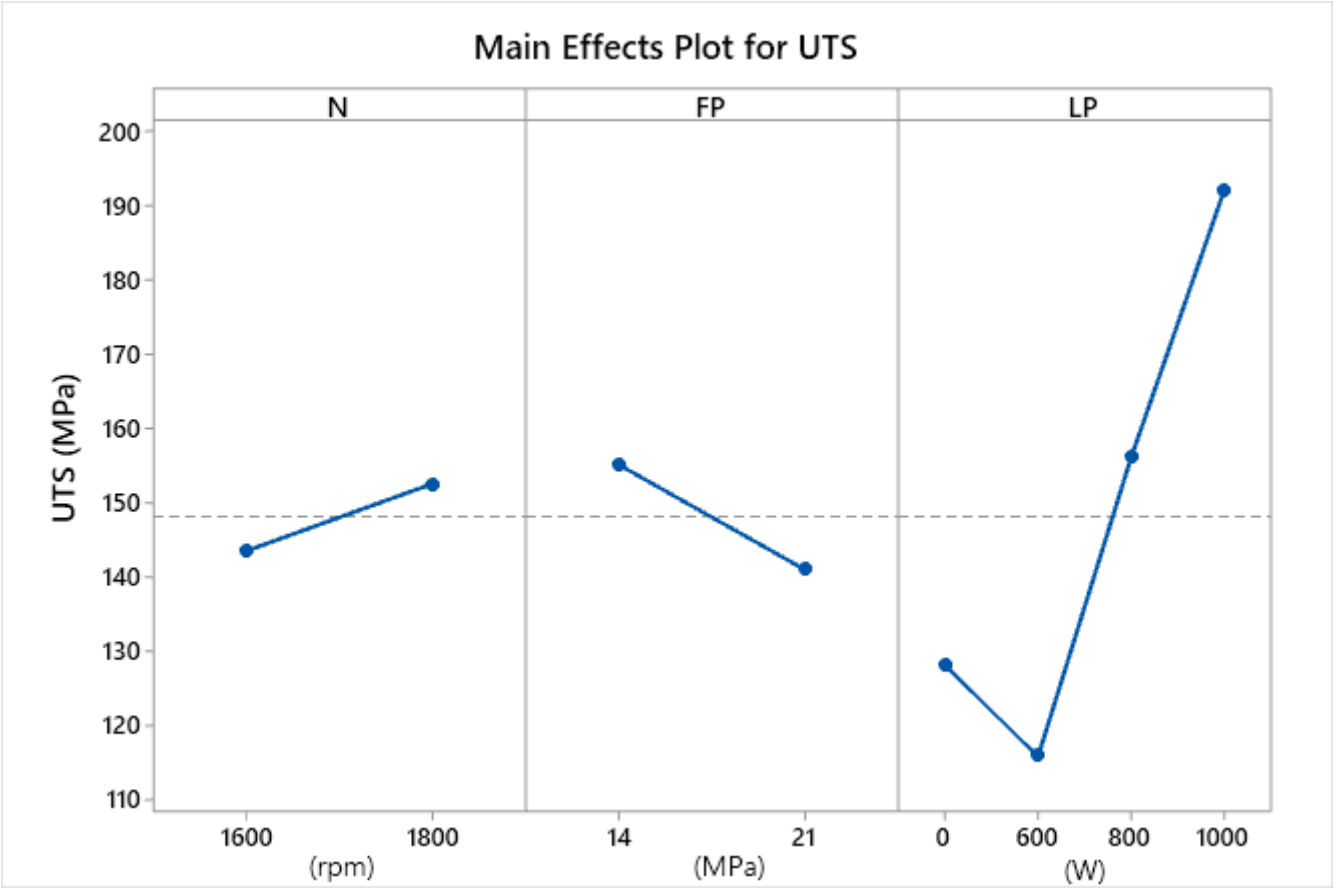

Figure 5

Main effects of experimental factors on the UTS

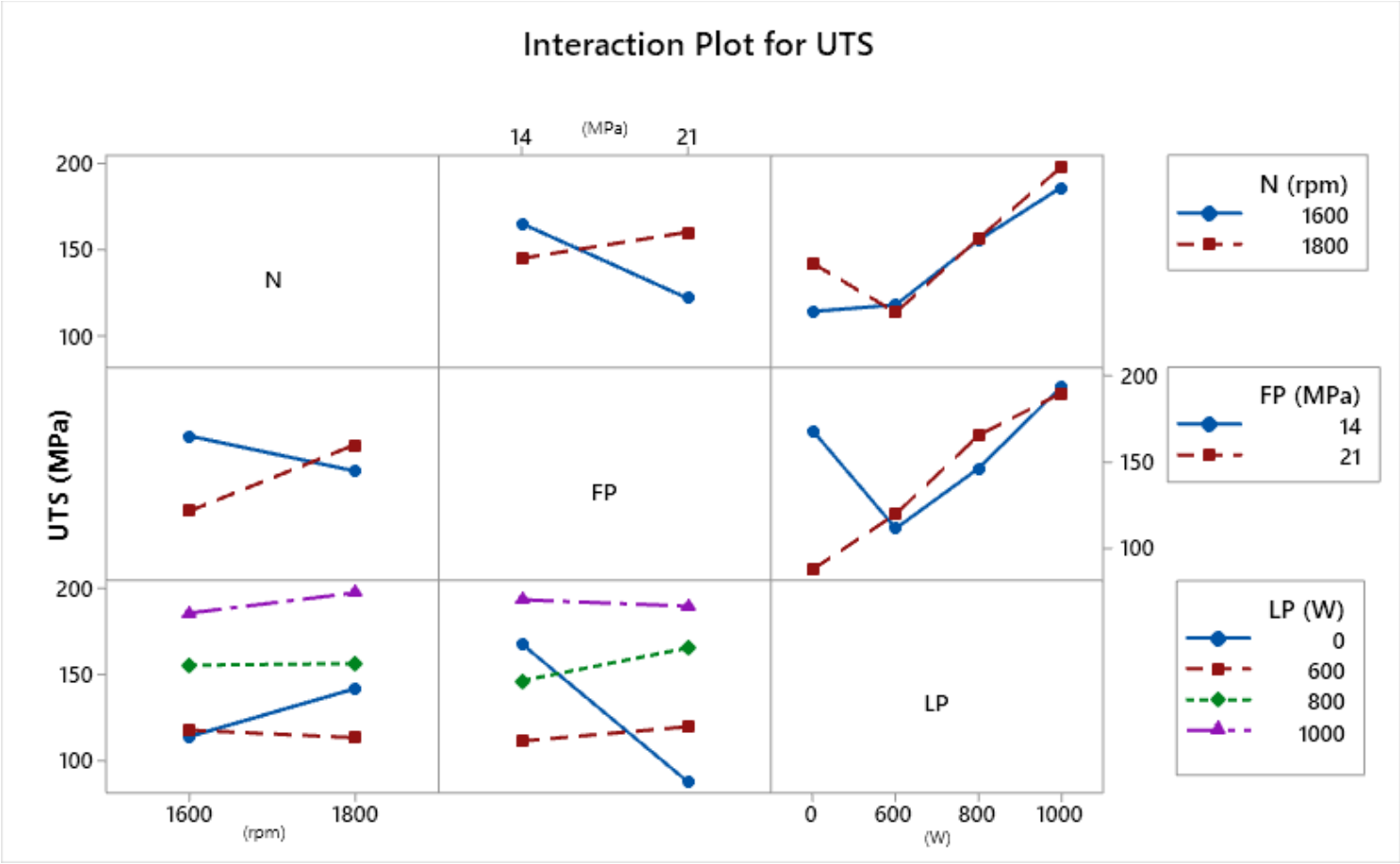

Figure 6

Interaction plot of factors on the overall UTS

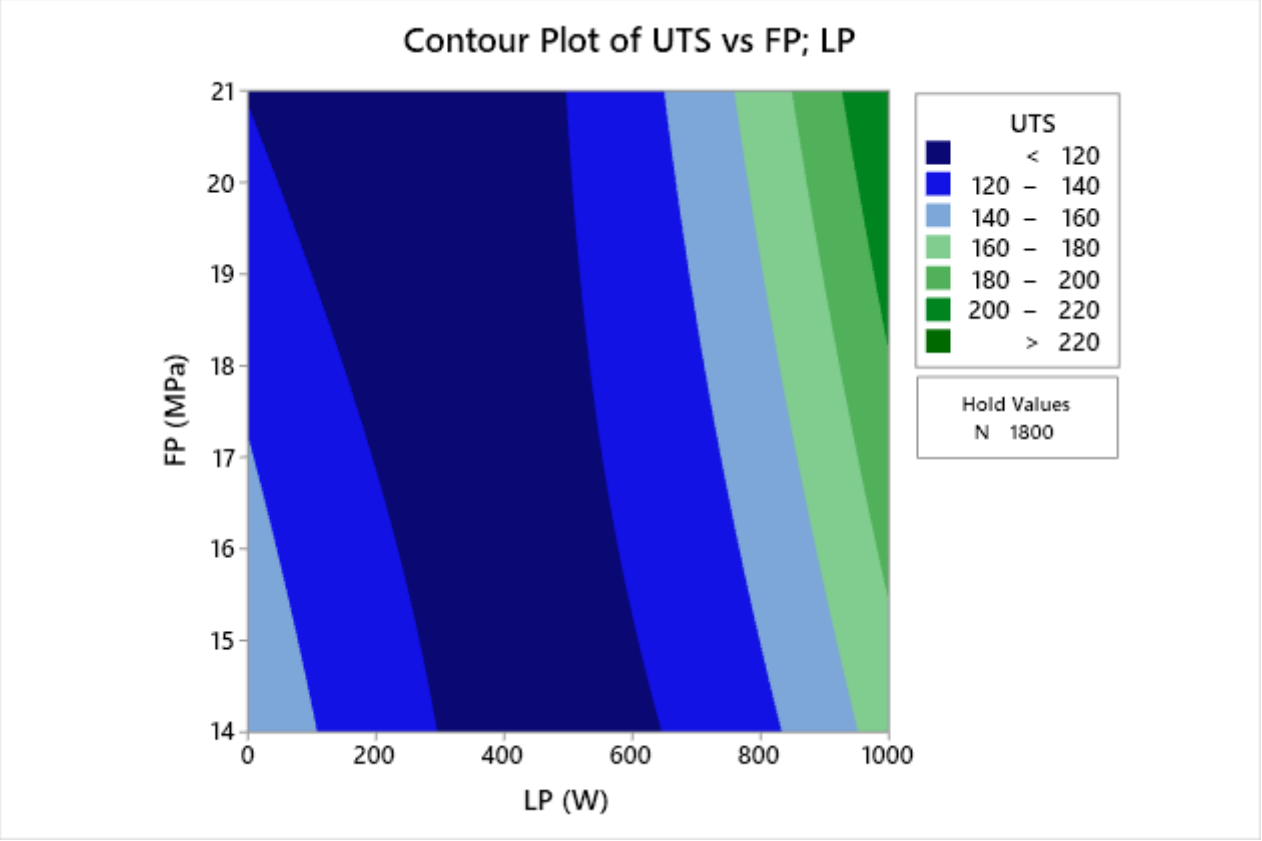

Figure 7

Contour plot of interaction between laser power and friction pressure

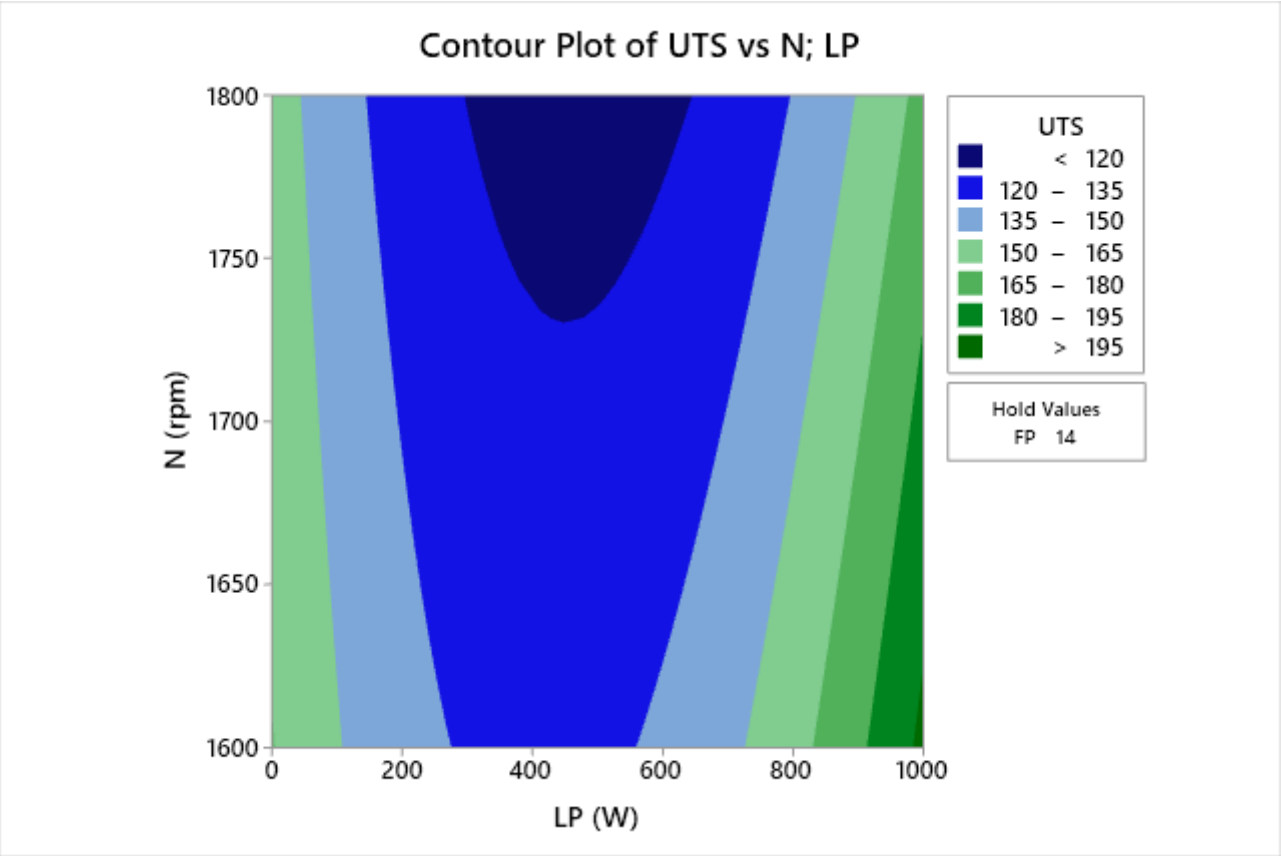

Figure 8

Contour plot of interaction between laser power and rotational speed

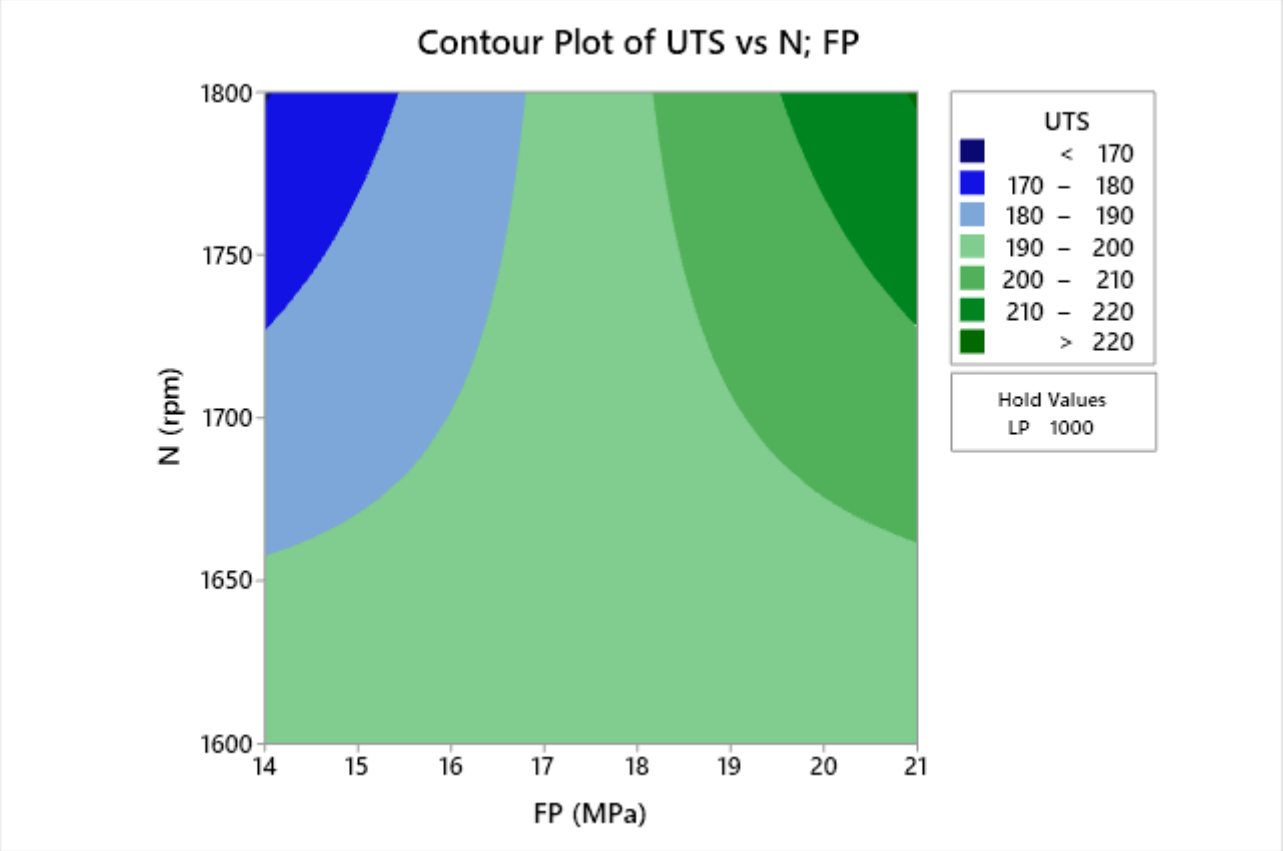

Figure 9

Contour plot of interaction between friction pressure and rotational speed

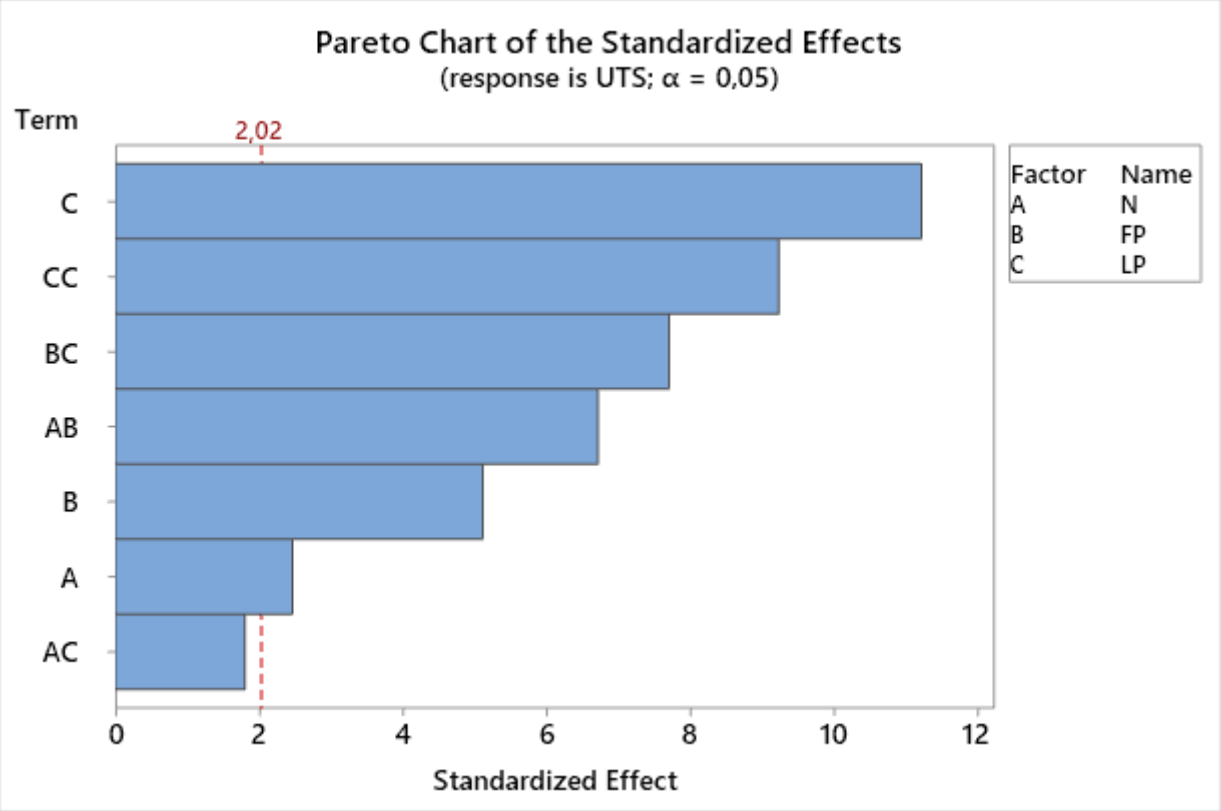

Figure 10

Pareto chart of the standardized effect

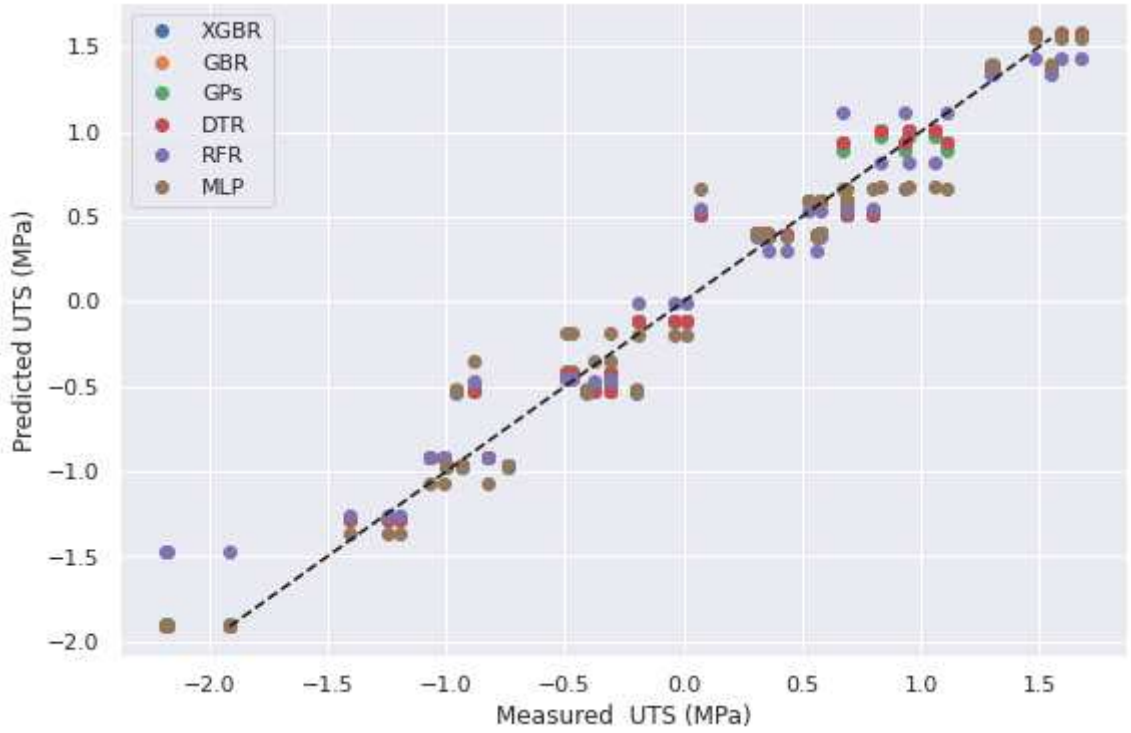

Figure 11

Scatter plot for comparing ML regressors accuracy in the UTS prediction

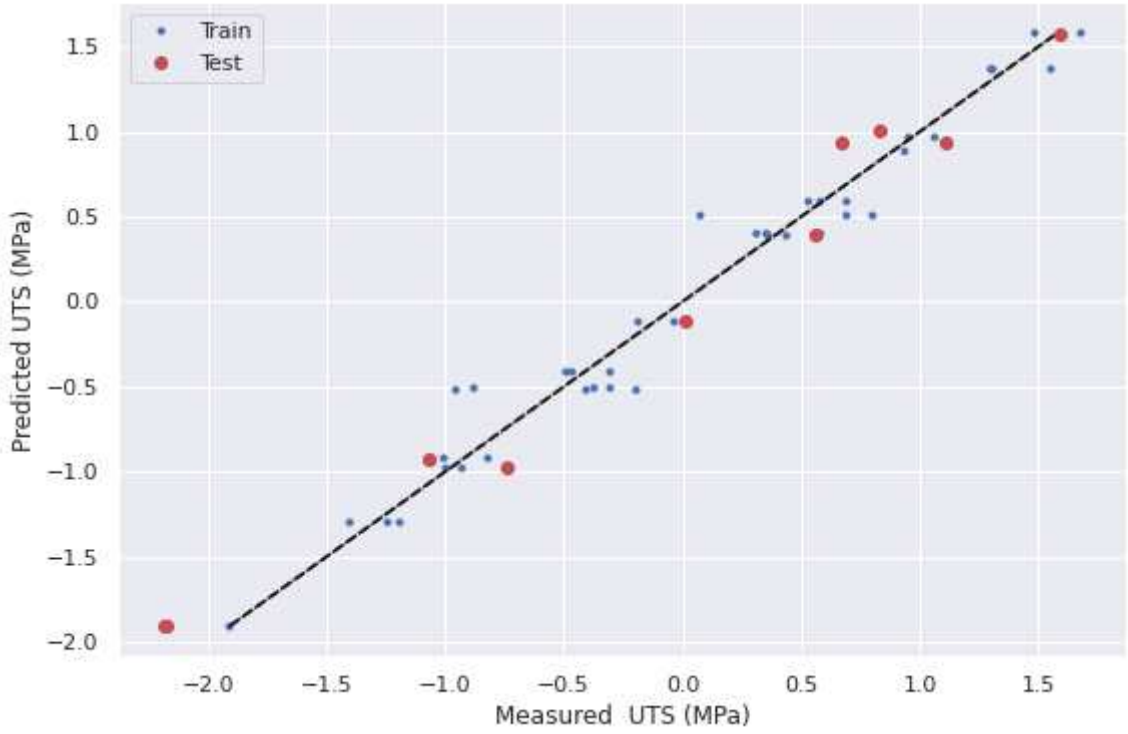

Figure 12

Scatter plot for accuracy evaluation of the GBR performance in the UTS prediction

```
Feature: 0, Score: 0.09419
Feature: 1, Score: 0.28351
Feature: 2, Score: 0.62230
```

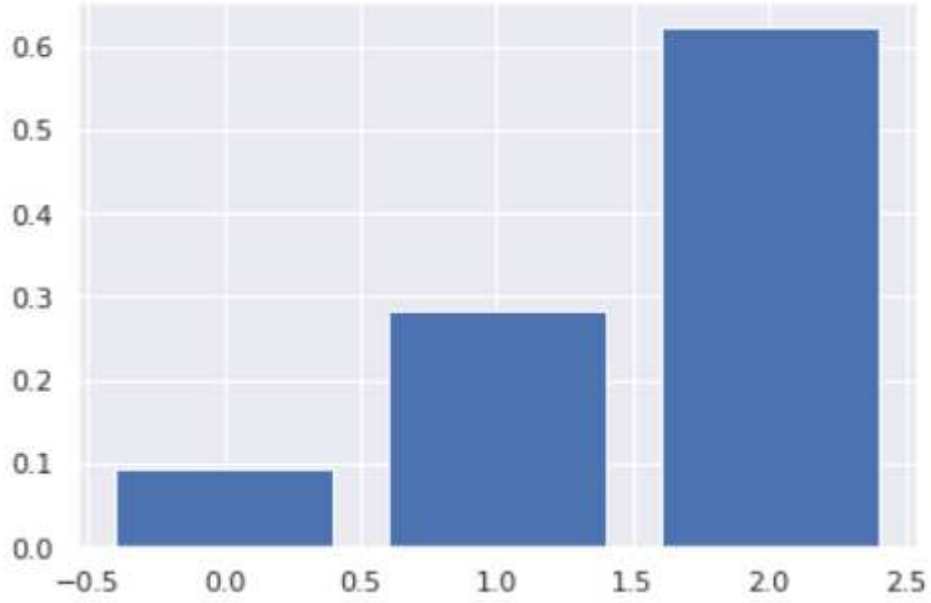

Figure 13

Feature importance analysis of the processing parameters in LARFW